Quantum suppression of chaotic tunnelling

2007 J. Phys. A: Math. Theor. 40 F397

(http://iopscience.iop.org/1751-8121/40/21/F01)

IOP FTC
IOP PUBLISHING JOURNAL OF PHYSICS A: MATHEMATICAL AND THEORETICAL

J. Phys. A: Math. Theor. **40** (2007) F397–F405 doi:10.1088/1751-8113/40/21/F01

FAST TRACK COMMUNICATION

Quantum suppression of chaotic tunnelling

Akiyuki Ishikawa, Atushi Tanaka and Akira Shudo

Department of Physics, Tokyo Metropolitan University, Minami-Osawa, Hachioji, Tokyo 192-0397, Japan

Received 19 February 2007, in final form 6 April 2007
Published 8 May 2007
Online at stacks.iop.org/JPhysA/40/F397

Abstract
The interplay between chaotic tunnelling and dynamical localization in mixed phase space is investigated. Semiclassical analysis using complex classical orbits reveals that tunnelling through torus regions and transport in chaotic regions are not independent processes, rather they are strongly correlated and described by complex orbits with both properties. This predicts a phenomenon analogous to the quantum suppression of classical diffusion: chaotic tunnelling is suppressed as a result of dynamical localization in chaotic regions. This hypothesis is confirmed by numerical experiments where the effect of destructive interference is attenuated.

PACS numbers: 03.75.Lm, 05.45.Mt, 03.65.Sq, 05.45.−a

(Some figures in this article are in colour only in the electronic version)

Tunnelling phenomena are purely quantum effects. Nevertheless, its nature is strongly influenced by underlying classical dynamics. In particular nontrivial aspects appear in the dynamical tunnelling in mixed-type phase space, in which quasi-periodic and chaotic trajectories coexist [1]. Tunnelling transitions between quasi-doublet states are enhanced by chaotic states [2] and the existence of nonlinear resonances also leads to a qualitative change of tunnelling processes [3, 4]. The problem of quantum tunnelling in multidimensional systems or more specifically in nonintegrable systems first raised in [5] would be of fundamental importance in quantum mechanics, and an approach taken there has recently been extended in [6]. However, our understanding for multidimensional tunnelling is still far from complete. A primary difficulty lies in the fact that dynamical tunnelling in chaotic systems takes place in a very complicated phase space; the structure of the classical phase space itself is not an easily understandable object. Another reason would be that dynamical tunnelling proceeds in complex environments in the sense of wave phenomena. Scarring [7] or dynamical localization [8, 9], or other types of invariant structures become sources of partial structures often observed in wavefunctions. It is not clear at all to what extent these various wave effects are independent of each other. These aspects make it difficult to evaluate the tunnelling rate between torus to chaotic regions quantitatively.

The trajectory description would be one of the promising strategies to understand quantum phenomena of chaotic systems. In particular, the semiclassical analysis is now recognized as an efficient approach to this end, and there are indeed a bunch of numerical tests supporting its validity. Concerning dynamical tunnelling, it was shown that the complex semiclassical theory works fairly well and explains the mechanism of tunnelling penetration out of quasi-periodic regions to chaotic seas [10–12]. In such a treatment, the classical dynamics is extended to complex phase space, and the trajectories on the Julia set are most responsible for reproducing tunnelling wavefunctions [13].

The aim of the present letter is, based on the arguments predicted by the complex trajectory description of chaotic tunnelling, to show that dynamical tunnelling in mixed phase space and dynamical localization are strongly correlated to each other, so that the destruction of coherence, or more precisely the destruction of destructive interference in chaotic regions, not only induces delocalization of wavefunction in chaotic regions, but also causes strong enhancement of tunnelling transition. In other words, 'genuine' chaotic tunnelling is suppressed by dynamical localization in surrounding chaotic regions, which is entirely an analogous mechanism as dynamical localization suppresses classical diffusion [8, 9]. The result must serve as further understandings of *amphibious states* [14, 15], recently discovered quantum states that show the failure of semiclassical wavefunction hypothesis [16].

We first provide evidence for why we can predict that chaotic tunnelling is tightly correlated with the dynamical localization process. As found in [11, 13], an exponentially large number of complex orbits appear as the contributors of the time-domain semiclassical propagator, and they indeed have almost equal weights in the semiclassical sum, which means that chaotic tunnelling occurs as a consequence of superposition of exponentially many component waves. To demonstrate it, we here employ an area-preserving map

$$F : \begin{pmatrix} p' \\ q' \end{pmatrix} = \begin{pmatrix} p - V'(q) \\ q + T'(p') \end{pmatrix} \tag{1}$$

where

$$T'(p) = ap + \tfrac{1}{2}(d_1 - d_2) + \tfrac{1}{2}[ap - \omega + d_1]\tanh b(p - p_d) + \tfrac{1}{2}[-ap + \omega + d_2]\tanh b(p + p_d) \tag{2}$$

$$V'(q) = -K \sin q. \tag{3}$$

As illustrated in figure 1(*d*), the phase space is divided into quasi-periodic and chaotic regions for $b \gg 1$. The kinetic term is almost linear for $|p| < p_d$, and tends to the standard map for $|p| > p_d$. The parameters d_1 and d_2 were put in order to get rid of small island structures which may appear around the border between the torus and chaotic regions. The smoothing factor tanh is introduced to allow analytical continuation of the map into complex plane.

The wavepacket launched at $p = 0$ goes out of the torus region due to tunnelling effects. Time evolution is described by the propagator in p-representation $\langle p_n|U|p_0\rangle$ and its leading-order semiclassical approximation takes the form

$$U^{sc}(p_0; p_n) = \sum_k A_k(p_0, p_n) \exp\left\{\frac{\mathrm{i}}{\hbar} S_k(p_0, p_n)\right\}, \tag{4}$$

where the summation is taken over all classical paths k satisfying given initial and final momenta, $A_k(p_0, p_n)$ and $S_k(p_0, p_n)$ stand for the amplitude factor associated with the stability and the corresponding classical action, respectively.

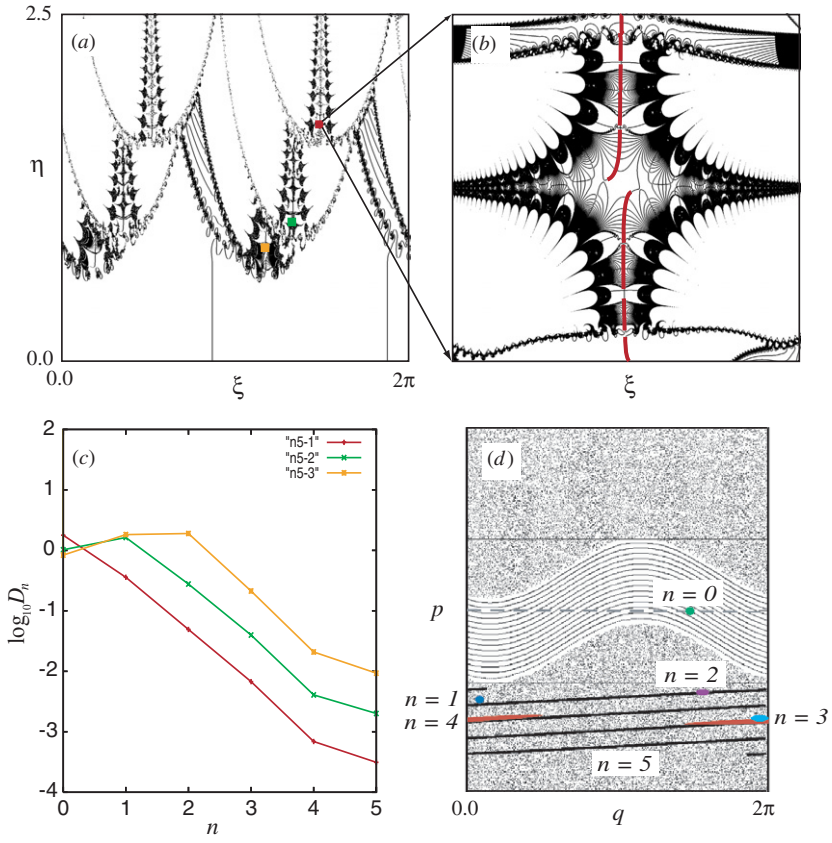

Figure 1. (*a*) A set of initial conditions $\mathcal{M}_n^\alpha$ ($\alpha = 0$), and (*b*) its magnification. Bold lines are parts of chained structures which substantially contribute to the semiclassical propagator (4). $|\mathrm{Im}\, q_n|$ of such orbits are very small. The parameters are chosen as $n = 5$, $a = 5$, $b = 100$, $d_1 = -24$, $d_2 = -26$, $\omega = 1$, $p_d = 5$ and $K = 2$. (*c*) The distance from the real plane ($D_n = \sqrt{|p_n|^2 + |q_n|^2}$) as a function of time step, where p_n and q_n denote (p, q) at n. The initial conditions are taken from the points indicated in (*a*). Note that the orbits whose initial imaginary parts are small (square and cross) do not necessarily go to the real plane directly, rather take a side trip in complex phase space. (*d*) The Lagrangian manifold projected onto real phase space. Here the Lagrangian manifold refers to $F^n(M_n^\alpha)$, and the initial conditions giving these manifolds shown in (*d*) are bold lines shown in (*b*). The dot (labelled as $n = 0$) represents the initial condition and curves (labelled as $n = 5$) is the final Lagrangian manifold.

For given $\alpha \in \mathbb{R}$, we have a set for initial conditions of semiclassically contributing complex paths as

$$\mathcal{M}_n^\alpha \equiv \{(p_0, q_0 = \xi + \mathrm{i}\eta) \in \mathbb{C}^2 \mid p_0 = \alpha,\ p_n \in \mathbb{R}\}. \tag{5}$$

As shown in figures 1(*a*) and (*b*), there exist a bunch of complex trajectories that satisfy the boundary conditions imposed on the initial and final steps. The set $\mathcal{M}_n^\alpha$ is composed of strings, each of which corresponds to the contribution k in the sum (4). In the case of the present map, the number of strings is infinite even for a finite fixed time step, reflecting that the map contains transcendental functions, while only finitely many complex orbits appear in the case of the map composed of polynomial functions. What was found in [11, 13] is, irrespective of the form of maps, that the tunnelling wavefunction is well controlled and quantitatively reproduced by

special types of complex orbits. Such orbits appear as a chained structure in the set $\mathcal{M}_n^{\alpha}$, an example of which is displayed in figure 1(*b*). The orbits forming chained structures are shown in red colour. It was also shown in [11, 13] that the number of complex orbits substantially controlling the tunnelling process increases as a function of time. Further important features actually shown here are that all these approach the real plane exponentially. These are both explained by the fact that such orbits are attracted by unstable periodic orbits on real plane [24]. All the stable manifolds of unstable periodic orbits extended to complex plane in general reach and intersect an initial state $(p_0, q_0 = \xi + \mathrm{i}\eta) \in \mathbb{C}^2$, thereby the orbits launched at the initial state go out of regular regions by following stable manifolds and approach the real plane exponentially.

It is important to note that, after reaching quasi-real regions, the dynamics of complex orbits is almost governed by the real dynamics. Figures 1(*c*) and (*d*) plot the distance from the real plane, and the projection of final manifolds onto the real plane, respectively. Three curves shown in figure 1(*c*) show the itinerary of complex orbits staring at three initial points marked in figure 1(*a*). Note that each one is not the itinerary of a single orbit, but a representative of an exponentially large number of orbits around each initial point, since these initial points are very close to each other. For example, the orbits starting at the red part in figure 1(*b*) behave in the same way as the red curve in figure 1(*c*), so these are not distinguishable from each other.

Along the final manifold presented in figure 1(*d*), $|\mathrm{Im}\, q_n|$ is very small, meaning that it almost follows the stretching and folding mechanism in real phase space. We notice that, within a single step, the orbits already go out from the torus region, and then go down to the real plane exponentially with being stretched in the unstable direction. In the final step ($n = 5$ in this case), the stretched manifold is almost real. Therefore, if one focuses on the manifold contained in the chaotic regions, the situation is almost the same as what is taking place in real dynamics. In this way, complex orbits controlling chaotic tunnelling bear an *amphibious character* : running through the torus region in purely imaginary space, and extending over the quasi-real chaotic region.

Now recall that the wavefunction in chaotic regions is dynamically localized [8]. Although the semiclassical interpretation of dynamical localization is not still clear [17], it may be at least true that, if the semiclassical description works, the orbits contributing to the semiclassical sum (4) should have appropriate correlations among them [18]; otherwise, classical diffusion will be restored since the random phase in the semiclassical sum (4) cancels the off-diagonal contributions. In the present situation, it would be natural to expect that the quasi-real orbits discussed above are correlated in chaotic regions as well.

To check this speculation, we add noise to the chaotic region and destroy the coherence predicted here. The experiment is done by putting the noise term to the kinetic term (2) as

$$T'(p) = T_0'(p) + \zeta T'_{\mathrm{noise}}(p). \tag{6}$$

Here $T_0'(p)$ represents the kinetic term (2), and ζ a stochastic variable obeying the Gaussian distribution with a variance ε. As schematically shown in figure 2(*a*), setting $T'_{\mathrm{noise}}(p) = 1$ for $|p| \geqslant L$, $= 0$ for $|p| < L$, we apply noise only in the region $|p| \geqslant L$. To see the tunnelling amplitude, we will monitor the probability P_n^{torus} defined as

$$P_n^{\mathrm{torus}} = \int_{p_a}^{p_b} |\psi_n(p)|^2 \, \mathrm{d}p, \tag{7}$$

where $\psi_n(p)$ represents the wavefunction at time step n, which is initially placed at $p_0 = 0$, and p_a and p_b are the coordinates specifying the minimum and maximal values of the torus region projected onto the p-axis (see also figure 1(*d*)). Here, we imposed the periodic boundary condition in the p-direction. As shown in figure 2(*a*), wavefunction outside the torus region

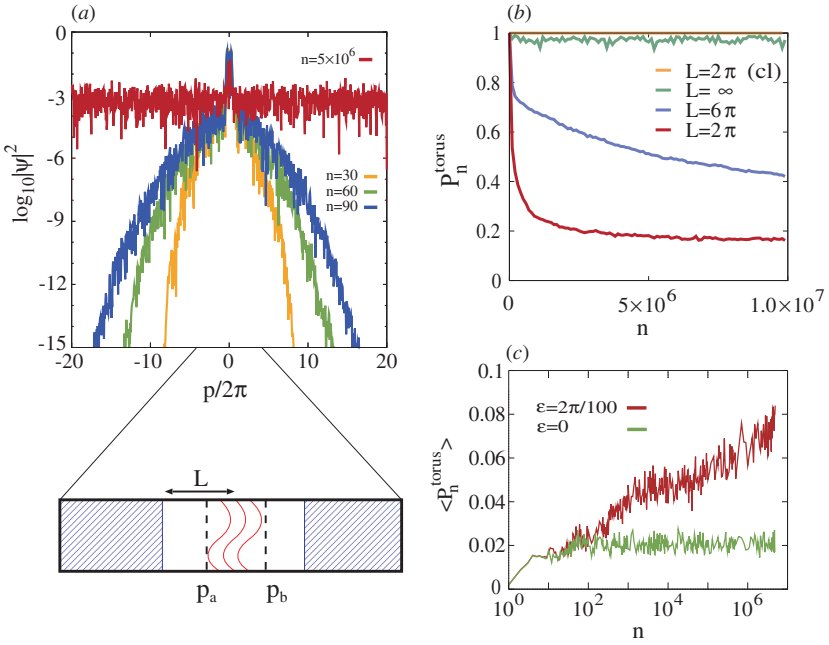

Figure 2. (a) Time evolution of wavepacket launched at $p_0 = 0$ state. Noise is applied only in the hatched regions in the schematic picture of phase space. $a = 4+0.1\sqrt{3}$, $\omega = 2\pi(1+\sqrt{7})/10$, $d_1 = -ap_d + \omega$, $d_2 = -ap_d - \omega$, $p_d = \pi$, $L = 2\pi$, $|p_a - p_b| = 1.6\pi$, $N = 1000$ and $\hbar = 0.1\pi$, where N denotes the system size. The noise intensity is given as $\varepsilon = 0.1\pi$. (b) P_n^{torus} as a function of time step n. The parameter values are the same as (a). Note that $P_{\text{eq}}^{\text{torus}} = 0.016$ is far below a saturated value for the case $L = 2\pi$. (c) The probability inside the torus region P_n^{torus} as a function of n for the cases without noise ($\varepsilon = 0.0$) and with noise ($\varepsilon = 2\pi/100$). The initial wavepacket is set as $\psi_0(p) = A\exp(2\pi i\eta(p))$ (for $|p| \geqslant 2\pi$), $= 0$ (otherwise). Here A is a normalization constant, and $\eta(p)$ = uniformly random in [0, 1]. The plot is given after averaging over ten ensembles with respect to the phase $\eta(p)$.

spreads as time proceeds and the profile of its tail shows that the classical diffusion process is recovered due to the destruction of interference which causes dynamical localization [19, 20]. Figure 2(b) plots P_n^{torus}, clearly demonstrating a drastic enhancement of tunnelling probability. Note that the ensemble of real classical orbits whose initial distribution is set to be the same as the quantum initial distribution almost stays inside the torus region and does not leak out even under the same noise. We can see that with the increase of L, which makes the chaotic region surrounding the torus region large, the tunnelling rate decreases. As will be reported elsewhere [23], extensive computations reveal that the exponent obtained by fitting an exponential function to the initial decaying interval of P_n^{torus}, up to 10^4 or 10^5 in the case of figure 2(b), decreases monotonically as a function of L. These are consistent with our interpretation that the presence of localized regions suppresses potentially existing tunnelling amplitude, which is related to an exponentially large number of complex orbits shown in figure 1. At the same time, note that the noise average is not necessary for the enhancement of the tunnelling: figures 2(a) and (b) are such examples.

An important remark would be that the tunnelling leakage continues but its rate γ could not be fitted by a simple exponential function in the whole time scale. The rate of penetration slows down with time and it takes very long time, if so, to reach the equilibrium state. If

the wavepacket spreads over phase space equally, the final probability should take the value $P_{\rm eq}^{\rm torus} = 0.016$, which is estimated under the assumption that the wavepacket is uniformly distributed over the phase space. (Note again that the phase space in the experiment is compact since periodic boundary conditions are imposed on both directions.) However, $P_n^{\rm torus}$ is still far above $P_{\rm eq}^{\rm torus}$, and the localized peak around the torus region remains, meaning that the wavepacket does not spread over phase space in an equal weight even after sufficiently long time.

Since an exponentially large number of complex paths exist also from the chaotic region to the torus region [13], the inverse tunnelling process should be enhanced as well. Indeed, as shown in figure 2(*c*), if we place the initial wavepacket in the chaotic sea, instead of the torus region, the tunnelling flow into the torus region is also highly enhanced with noise being applied on chaotic seas. This result tells us that the chaotic region with external noise does not work merely as a sink or reservoir. If this is the case, the unidirectional flow from the torus to chaotic regions is expected to take place and the tunnelling back process should not be observed.

Similar strong enhancement is observed when we design the system so that the wavepacket moves freely in the regions $|p| \geqslant L$. The motivation to put ballistic regions is again in order to get rid of dynamical localization, as the case where noise is applied. To realize it, we replace the kinetic term (2) by

$$T'(p) = \tfrac{1}{2}ap\{\tanh b(p+L) - \tanh b(p-L)\} + \tfrac{1}{2}(ap-\omega)\{\tanh b(p-p_d) - \tanh b(p+p_d)\}. \tag{8}$$

The parameter L controls the border from which the ballistic propagation begins to occur. Furthermore, to avoid the recurrence of the wavepacket to the initial domain, we put the absorbing boundary at $|p| = p_{\rm cutoff}$. More precisely, a projection operator $\hat{P}$, which satisfies $\langle p|\hat{P}|\psi\rangle = 0$ for $|p| > p_{\rm cutoff}$, and $\langle p|\hat{P}|\psi\rangle = \langle p|\psi\rangle$ for $|p| < p_{\rm cutoff}$, is applied in each time step. After penetrating through the torus region, the wavepacket propagates in chaotic seas up to $|p| \simeq L$. Then it moves ballistically in the region $|p| > L$ and is absorbed at $|p| = p_{\rm cutoff}$. Note that the original map (2) is recovered in the limits $L \to \infty$ and setting $d_1 = d_2 = 0$.

We launch the wavepacket from the centre of the torus region $p_0 = 0$ and observe the same quantity $P_n^{\rm torus}$ introduced above. As shown in figure 3, the enhancement of tunnelling amplitude is again remarkable as compared to the system without outside ballistic propagation. We further note that, as seen in figure 3(*a*), although the amplitude of wavefunction on the torus region is gradually reduced as a result of tunnelling leakage, it is still distinguishably localized on the torus region. Figure 3(*b*) also exhibits that $P_n^{\rm torus}$ remain finite after exceedingly long time steps. Especially in cases of $L = 2\pi$ and $L = 4\pi$, even a signature of saturation can be detected.

To see that the observed process is certainly a chaos-involved one, in other words, not only the localization length but also the nature of chaos, especially the strength of chaos controls the transition amplitude, we change the nonlinear parameter K in our system. Taking into account that the localization length is proportional to K^2 [21], we plot in figure 4 the tunnelling rate γ as a function of K for several scaled values $\bar{L} = L/K^2$. In this experiment, the initial wavepacket is again placed inside the torus region. The kinetic term is replaced by

$$T'(p) = \tfrac{1}{2}a(p-p_d) + \omega + \tfrac{1}{2}a(p-p_d)\tanh b(p-p_d), \tag{9}$$

which gives phase space whose lower part ($p < 0$) is all covered with KAM circles. The kinetic term (9) is obtained by letting the second $p_d \to \infty$ and putting $d_1 = -ap_d + \omega$. Such manipulation is necessary to avoid the wavepacket penetrating through the KAM domains and reaching the opposite chaotic region. The result shows that the degree of

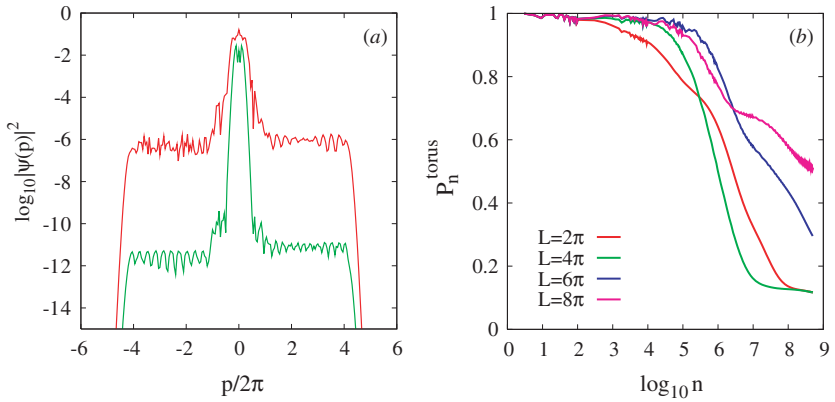

Figure 3. (*a*) The wavefunction $|\psi_n(p)|^2$ at a relatively short ($n = 3000$) and a sufficiently long time step ($n = 2 \times 10^8$) in the case of the map with the kinetic term (8) with $a = 4.071$, $\omega = 2.4575$, $N = 400$, $L = 2\pi$ and $\hbar = 1/40\pi$. Both are averaged over 100 steps around each time step. The absorbing boundary is set at $p = \pm 8\pi$, and the ballistic motion occurs in the blue region in the schematic phase space depicted in figure 2(*a*). (*b*) Long time behaviour of P_n^{torus} for various L.

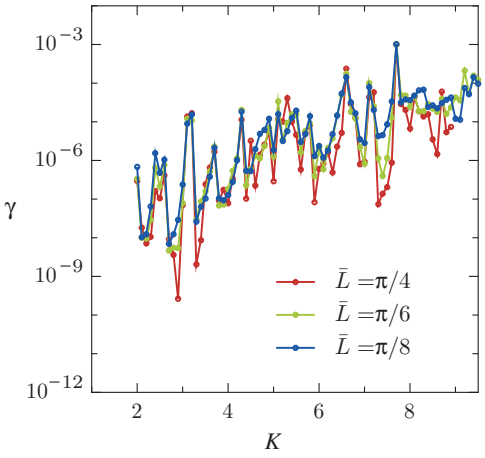

Figure 4. The tunnelling rate γ as a function of the kicking strength K. γ is evaluated by fitting the initial decay of P_n^{torus} for $n < 10^4$ or 10^5 depending on K. The length L of the chaotic region without noise (see figure 2(*a*)) is scaled as $\bar{L} = L/K^2$. Here $p_d = 0.6\pi$, $a = 4 + 0.1\sqrt{3}$ and $\omega = 2\pi(1 + \sqrt{7})/10$.

enhancement depends on the strength of chaos. Our interpretation for the result is that the density of stable and unstable manifolds becomes large with the increase of K, the number of complex paths responsible for the tunnelling transition increases, which yields large tunnelling amplitude.

These numerical tests, together with the semiclassical analysis using complex trajectories show that chaotic tunnelling and dynamical localization are strongly correlated. If the interference yielding dynamical localization is destroyed, potentially existing tunnelling trajectories show up, which leads to the drastic enhancement of tunnelling amplitude. This makes a sharp contrast to the system coupled with the heat bath, in which quantum tunnelling

is suppressed [22]. We can alternatively say that torus states are sustained by surrounding dynamical localization, otherwise they cannot stay localized on the torus. Hence, amphibious states found in [14, 15] can be interpreted exactly as the flooding of chaotic tunnelling trajectories.

An important nontrivial question still not clarified is the origin of life time of torus states or the tunnelling rate between regular and chaotic regions. It is not obvious what dynamical information is needed to specify it. In the semiclassical argument, Lyapunov exponents and the topological entropy of outside chaotic regions again become necessary ingredients since, as mentioned in the first part, dominant tunnelling orbits are controlled by unstable periodic orbits in chaotic regions.

It is natural to assume that inner torus states are more robust than the outer ones and the life time of the former is much longer than the latter [15]. This would be a qualitative explanation for slowing down phenomenon, but the problem looks more subtle. As shown in figure 1(c), the orbit shown by the red curve is launched at an inner torus as compared to the orbits shown by green and yellow curves (see ξ coordinate in figure 1(a) and also note that the initial condition is placed on $p_0 = 0$). Nevertheless, it gains smaller imaginary action Im S_n, since it approaches the real plane directly, whereas the latter two orbits launched at outer tori take side trips, which cause additional gains of Im S_n. This suggests the inner torus has a smaller life time than the outer one and so the tunnelling rate does not necessarily follow a simple order even in a clean setting as the present model.

It is also necessary to examine how the life time of (complex) classical orbits inside the torus region is related to the tunnelling rate. The initial manifold, $\{(p_0 = 0, \xi + \mathrm{i}\eta) \in \mathbb{C}^2\}$, represents the support of semiclassical wavefunction. It is found that the manifold starting at the region where the complex KAM domain dominates has a very long life time which has an entirely complex classical origin [24].

Acknowledgments

The authors thank R Ketzmerick and A Bäcker for their helpful comments. One of the authors (AS) is grateful to K S Ikeda for useful discussions.

References

[1] Bohigas O, Tomsovic S and Ullmo D 1993 *Phys. Rep.* **223** 43
[2] Tomsovic S and Ullmo D 1994 *Phys. Rev.* E **50** 145
[3] Brodier O, Schlagheck P and Ullmo D 2001 *Phys. Rev. Lett.* **87** 064101
Brodier O, Schlagheck P and Ullmo D 2002 *Ann. Phys., NY* **300** 88
[4] Mouchet A, Eltschka C and Schlagheck P 2006 *Phys. Rev.* E **74** 026211
[5] Wilkinson M 1986 *Physica* D **21** 341
Wilkinson M 1987 *Physica* D **27** 201
[6] Smith B C and Creagh S C 2006 *J. Phys. A: Math. Gen.* **39** 8283
[7] Heller E J 1984 *Phys. Rev. Lett.* **53** 1515
[8] Casati G, Chirikov B V, Ford J and Izrailev F M 1979 *Stochastic Behavior in Classical and Quantum Hamiltonian Systems* (Berlin: Springer) p 334
[9] Fishman S, Grempel D R and Prange R E 1982 *Phys. Rev. Lett.* **49** 509
[10] Creagh S C and Whelan N C 1996 *Phys. Rev. Lett.* **77** 4975
Creagh S C and Whelan N C 1999 *Phys. Rev. Lett.* **82** 5237
[11] Shudo A and Ikeda K S 1995 *Phys. Rev. Lett.* **74** 682
Shudo A and Ikeda K S 1998 *Physica* D **115** 234
Onishi T, Shudo A, Ikeda K S and Takahashi K 2001 *Phys. Rev.* E **64** 025201
[12] Takahashi K and Ikeda K S 2001 *Found. Phys.* **31** 177
Takahashi K, Yoshimoto A and Ikeda K S 2002 *Phys. Lett.* A **297** 370

[13] Shudo A, Ishii Y and Ikeda K S 2002 *J. Phys. A: Math. Gen.* **35** L225
[14] Hufnagel L, Ketzmerick R, Otto M-F and Schanz H 2002 *Phys. Rev. Lett.* **89** 154101
[15] Bäcker A, Ketzmerick R and Monastra A G 2005 *Phys. Rev. Lett.* **94** 054102
[16] Percival I C 1973 *J. Phys. B: At. Mol. Phys.* **6** L229
Berry M V 1977 *J. Phys. A: Math. Gen.* **10** 2083
Voros A 1979 *Stochastic Behavior in Classical and Quantum Hamiltonian Systems* (Berlin: Springer) p 326
[17] Kaplan L 1998 *Phys. Rev. Lett.* **81** 3371
[18] Shudo A and Ikeda K S 1994 *Prog. Theor. Phys. Suppl.* **116** 283
[19] Ott E, Antonsen T M Jr and Hanson J D 1984 *Phys. Rev. Lett.* **53** 2187
[20] Adachi S, Toda M and Ikeda K 1988 *Phys. Rev. Lett.* **61** 655
[21] Chirikov B V, Izrailev F M and Shepelyansky D L 1981 *Sov. Sci. Rev. Sect.* C **2** 209
Shepelyansky D L 1986 *Phys. Rev. Lett.* **56** 677
[22] Caldeira A O and Leggett A J 1981 *Phys. Rev. Lett.* **46** 211
[23] Ishikawa A, Tanaka A and Shudo A to be submitted
[24] Shudo A, Ishii Y and Ikeda K S to be submitted